Experimental and analytical study of flexural behaviour of BFRP sheets strengthened RC beams with new epoxy anchors

Cheng Yuan[1], Wensu Chen*[1], Thong M. Pham[1], Hong Hao*[1], Li Chen[2], Jun Wang[1]

[1] Centre for Infrastructural Monitoring and Protection, School of Civil and Mechanical Engineering, Curtin University, Australia

[2] School of Civil Engineering, Southeast University, China

*Corresponding Authors: wensu.chen@curtin.edu.au (W. Chen), hong.hao@curtin.edu.au (H. Hao).

Abstract

Intermediate crack (IC) debonding is a common failure mode of externally bonded (EB) FRP-strengthened RC beams. This debonding failure initiates at an intermediate crack and propagates towards a plate end. New epoxy anchor was proposed recently by the authors and has shown its effectiveness in enhancing interfacial bonding behaviour and therefore it might be effective to delay or suppress IC debonding failure in RC beams. This study is to experimentally investigate the efficiency of using epoxy anchors for mitigating the IC debonding under three-point bending tests. The application of the new proposed epoxy anchors has advantage of simple installation procedure including pre-drilling holes and then bonding FRP. Totally, five RC beams including one control specimen and four anchored ones were tested. Damage modes and structural response of unanchored and anchored RC beams were evaluated and discussed. The effects of various configurations of epoxy anchors were analysed and discussed. The experimental results show that the load-carrying capacity and the ductility of anchored beams increased by up to 13.12% and 53.31%, respectively, and the strain utilization of FRP can be significantly improved by 43.48% as compared to the control specimen.

Keywords: BFRP; Flexural strengthening; RC beams; IC debonding; Epoxy anchor.

1. Introduction

Fibre-reinforced polymer (FRP) has been widely used in the flexural strengthening of RC beams due to its high strength-to-weight ratio and excellent durable nature [1-3]. Despite the well reported benefits of EB FRP sheets for the strengthening, the brittle and premature debonding failure is the main drawback of the technique [4-6]. It is found that the intermediate crack (IC) debonding and plate end (i.e., concrete cover separation) debonding are the two common debonding failure modes in FRP-strengthened RC beams [7-9]. IC debonding is caused by an intermediate crack propagating from the mid-span to the plate end, while the concrete cover separation has the debonding failure starts from the plate end and passing to the mid-span [10]. Debonding of FRP as a premature failure mode reduces the efficient utilization of FRP composite as well as the effectiveness of strengthening [11-14].

Numerous anchorage systems have been proposed as mitigation measures to suppress debonding failure or postpone debonding process, such as FRP U-jacket anchors, FRP spike anchors, or mechanical anchors (i.e., steel fastener or anchor bolts) [15-18]. Among these proposed anchorage systems, the externally bonded (EB) FRP U-jacket anchors possess greater anchorage efficiency due to the ease of application and corrosion resistance [19-21]. Test results from wrapping transverse U-jacket anchors have shown an increase of 20% to 37.8% in flexural capacity of FRP-retrofitted concrete beams [22]. Laboratory study by Lee and Lopez [23] has shown that both shear resistance and debonding ductility of FRP-to-concrete joints can be enhanced by using 45° inclined FRP U-jacket. The inclined U-jackets were found to be effective in arresting flexural and shear cracks. It is also found that the vertical or 45° inclined FRP U-jackets are effective in moderating the concrete cover separation and intermediate crack debonding failure [24].

FRP spike anchorage system has been developed for EB strengthening, and the test results on FRP-to-concrete joints have shown that the debonding strength can be remarkably enhanced by the use of FRP spike anchors [25, 26]. Smith et al. [27] reported that both the load-carrying capacity and flexural strength were enhanced by 30% and 110%, respectively, for FRP-strengthened RC slabs. Tests on

FRP-to-concrete joints, which was designed to simulate the IC debonding, have shown that the increases of 50% to 80% in the interfacial shear resistance were achieved with various configurations of FRP spike anchors [28, 29].

Mechanical anchors have also been proposed to enhance the interfacial bond between FRP and concrete by improving the adhesion and friction [15, 30]. The mechanical anchors consist of steel plating, mechanical fasteners and adhesive [18, 31, 32]. The mechanical fastener at the interface pushes towards the anchor to generate a large normal pressure and therefore the frictional resistance [33]. Test results obtained by Wu and Huang [34] have shown that the bond strength of the strengthened RC beam with hybrid bonded FRP anchorage was approximately 8 times the bond strength of the specimen without anchorage. Tests on FRP-concrete interface have indicated that the debonding process was significantly postponed due to the extended debonding plateau [35].

However, the application of FRP U-jackets, FRP spike anchor or mechanical anchor increases the amount of FRP composites and costs more construction time [36]. To simplify the application procedure while enhance the interfacial bond, a new epoxy anchor was proposed by Yuan et al. [36] to postpone the debonding process. The development of epoxy anchors was inspired by the epoxy interlocking [37] and FRP spike anchor dowel action [38]. Test results [36] on the interfacial bond strength between FRP and concrete with epoxy anchors showed an increase of 77% and an increment of 87% in the effective utilization of FRP composite’s tensile strength. Due to the significant softening behaviour of epoxy resin during fracture, the debonding process can be remarkably extended. This study investigates the performance of this new epoxy anchorage system in strengthening concrete beams through three-point bending tests.

2. Experimental investigation

2.1 Design of RC beams

A total of five RC beams were prepared to study the efficacy of basalt-fibre reinforced polymer (BFRP) strengthening with epoxy anchors. The geometry and dimension of all the RC beams are detailed in Figure 1. As an extension of the previous study [22], the same reinforcement configuration was used in this study to examine the effectiveness of using new epoxy anchors. The dimensions of the beams were 250 mm in height, 150 mm in width and 2200 mm in length. Each beam was reinforced with two 12-mm-diameter tension steel bars and two 10-mm-diameter compression steel bars in the longitudinal direction. To ensure flexural-dominant behaviour, all the beams were designed with 10-mm-diameter steel stirrups at a spacing of 115 mm.

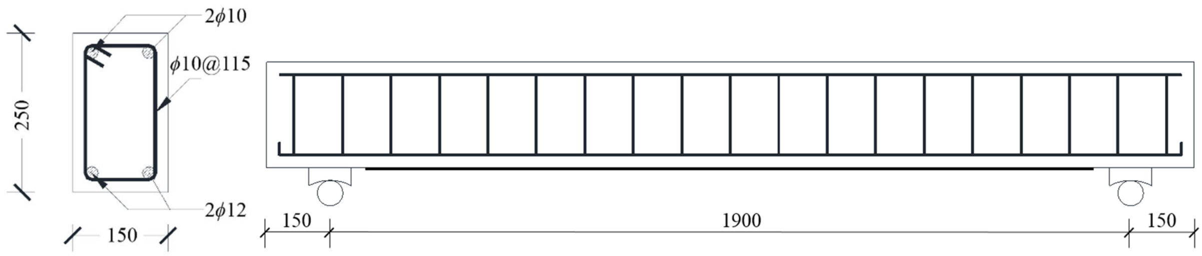

Figure 1. Dimensions of the test specimens (all dimensions in millimetres)

To investigate the effect of epoxy anchor configuration on the mitigation of FRP debonding, four anchorage schemes were employed as shown in Figure 2. One specimen (BC) served as the control beam, which was bonded with soffit FRP sheets without anchorage. Specimen BD_10_60 refers to the “Dense” anchorage with 10-mm-diameter epoxy anchors, anchorage spacing of 60 mm, and the total anchorage length of 1780 mm. Specimen BD_16_60 represents the “Dense” anchorage with 16-mm-diameter epoxy anchors, anchorage spacing of 60 mm, and the anchorage length of 1780 mm. Specimen BL_16_120 refers to the “Loose” anchorage with 16-mm-diameter epoxy anchors, anchorage spacing of 120 mm, and the total anchorage length of 1780 mm. Specimen BP_16_60 represents “Partial” anchorage area with the total anchorage length of 800 mm and 16-mm-diameter epoxy anchors and anchorage spacing of 60 mm.

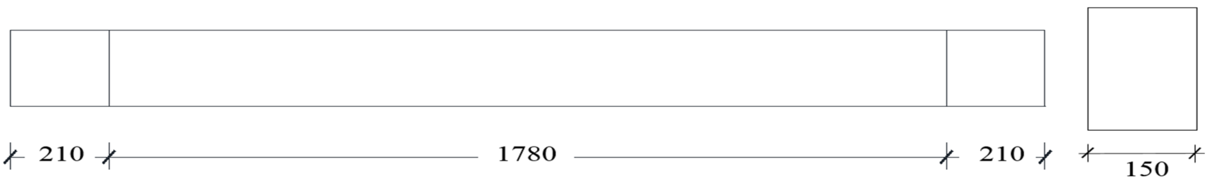

(a) Specimen BC

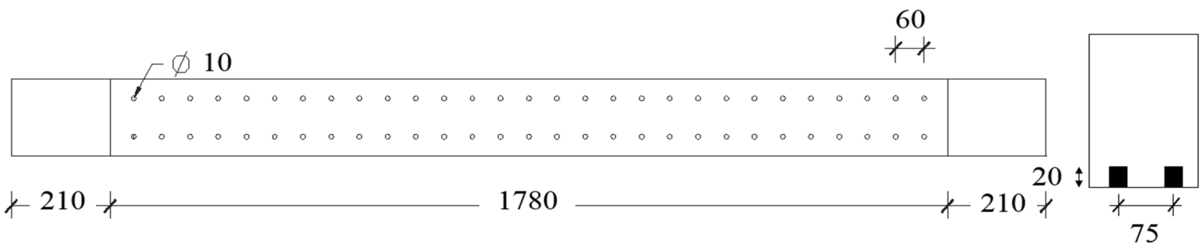

(b) Specimen BD_10_60

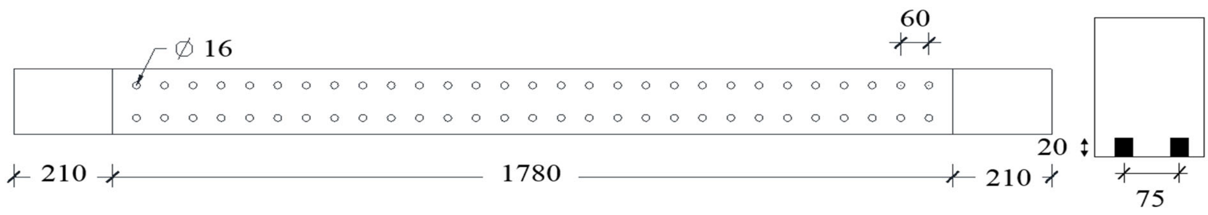

(c) Specimen BD_16_60

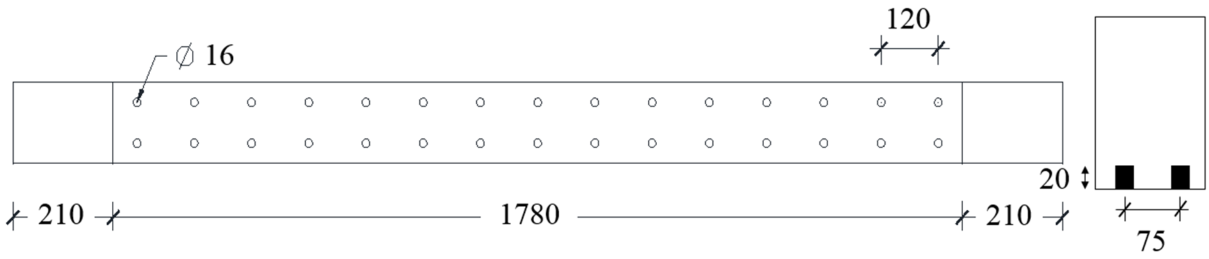

(d) Specimen BL_16_120

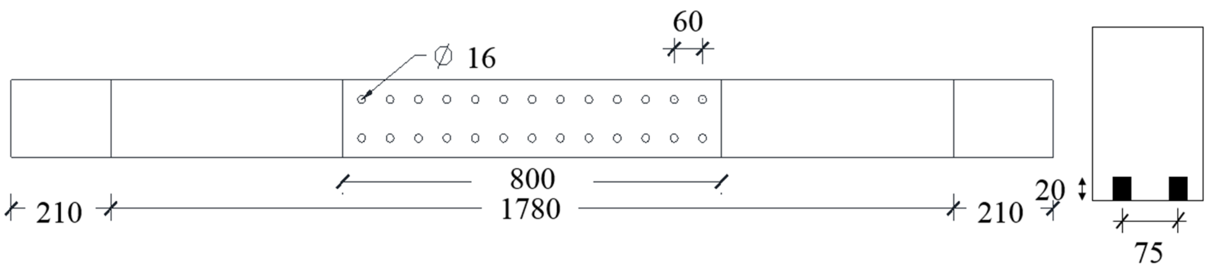

(e) Specimen BP_16_60

Figure 2. Epoxy anchor configurations of the tested beams (all dimensions in millimetres)

2.2 Specimen preparation

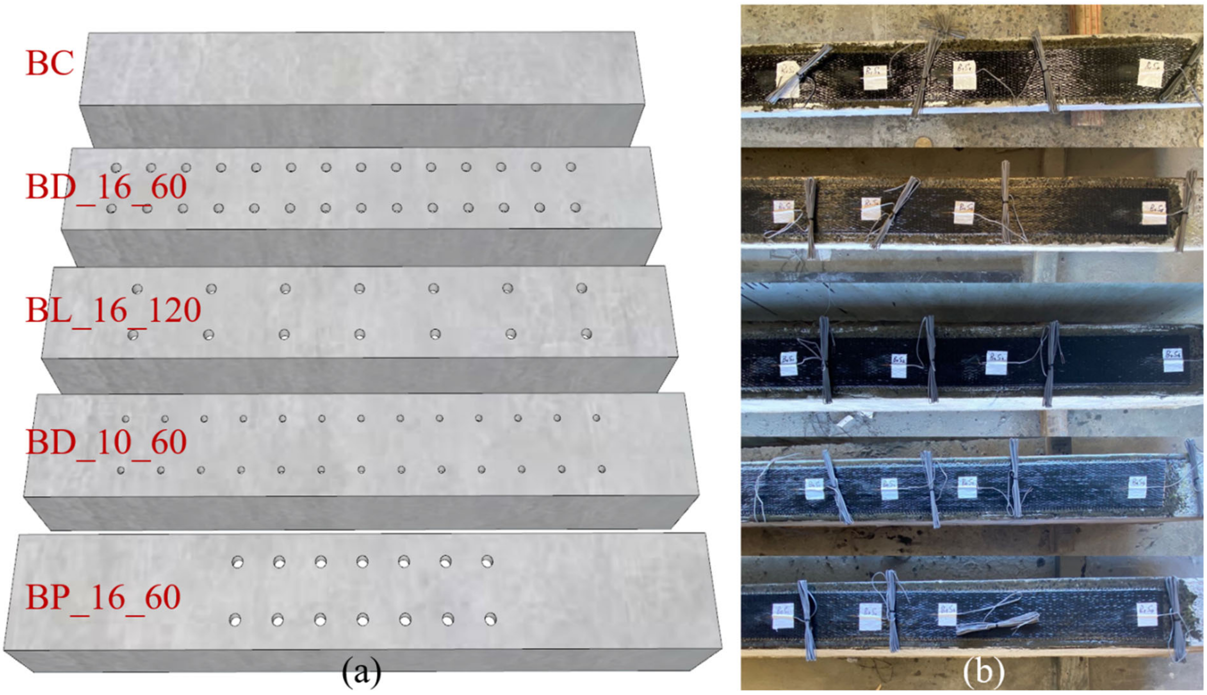

Figure 3. (a) Schematic diagram of anchor holes; (b) Test specimens

To ensure the consistent properties, all the beams were cast with the same batch of commercial concrete and cured under the same condition. After curing for 28 days, concrete surface for bonding of BFRP sheets was carefully roughened by a pneumatic needle gun to remove weak components. A hammer drill was used to drill the designed holes on the beams with a constant depth of 20 mm. The roughed surfaces along with the drilled holes were cleaned by a vacuum cleaner to remove dust and weak concrete caused by the process of needling and drilling. The holes were then filled with epoxy resin and the wet layup procedure was employed for BFRP sheet bonding. Four layers of unidirectional BFRP sheets were applied for all the beams. After preparation, the beams were cured for 7 days before flexural tests as detailed in Figure 3.

2.3 Material properties

As per the standard [39], the concrete for the beams had the average compressive strength (i.e., concrete cylinder with 100-mm-diameter and 200-mm-height) of 48.30 MPa and splitting tensile strength (i.e., concrete cylinder with 150-mm-diameter and 300-mm-height) of 3.56 MPa at 28-day.

The 100-mm-width unidirectional BFRP sheets with the density of 300 g/m^2 were used to externally reinforce the RC beams. The nominal thickness, tensile strength, elastic modulus, and rupture strain of the BFRP sheet was 0.12 mm, 2100 MPa, 77.9 GPa, and 2.1%, respectively. To ensure the occurrence of FRP debonding instead of FRP rupture, four layers of BFRP sheets were externally bonded to the soffit of RC beams. The adhesive consisting of epoxy resin and hardener at a volume ratio of 5:1 was used for epoxy anchor and BFRP sheets bonding. The adhesive had a tensile strength of 50.30 MPa, elastic modulus of 32 GPa, and failure strain of 4.5%.

2.4 Instrumentation and test setup

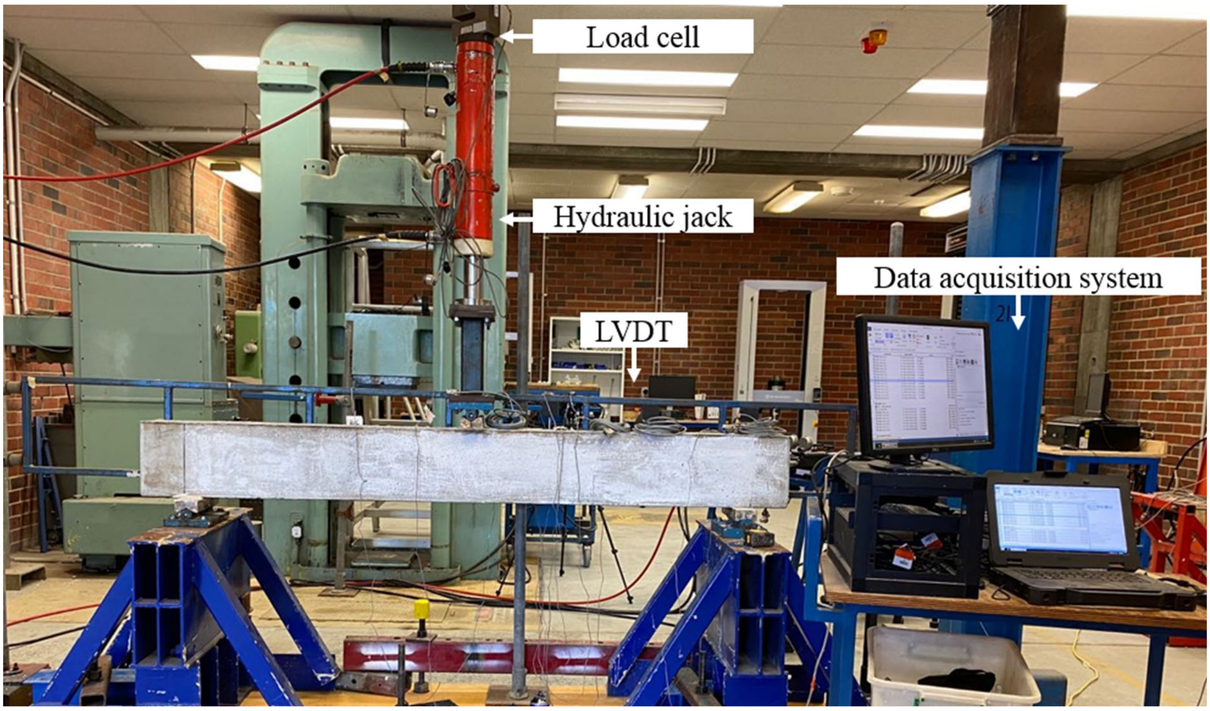

Figure 4. Test setup

Figure 4 illustrates the laboratory setup, which consists of a load cell, a hydraulic jack, linear variable differential transformers (LVDT), strain gauges, a data acquisition system, and a reaction frame. The loading was applied via a hydraulic jack. Three LVDTs were used to measure the deflections: one at the mid-span and two at the quarter span. Four strain gauges were attached to the BFRP surface to measure the FRP debonding strain at different locations, and the configurations of strain gauges are detailed in Section 3.

3. Test results and analysis

The experimental results of five beams are summarized in Table 1. The effects of epoxy anchor configurations on the ultimate load P_u, mid-span deflection at ultimate load δ_u, maximum strain of BFRP composite before debonding ε_{FRP}, strain utilization (i.e., utilization of nominal rupture strain capacity) of BFRP composite, and debonding failure mode were discussed and analysed. The load-deflection responses of all the beams are shown in Figure 5.

Table 1. Summary of experimental results

Specimen ID	Ultimate load P_u (kN)	Load increase (%)	Deflection at ultimate load δ_u (mm)	Maximum FRP strain ε_{FRP} (%)	Strain increment (%)	Strain utilization (%)
BC	99.48	/	22.38	1.38	/	65.71
BD_10_60	110.47	11.05	27.79	1.63	18.12	77.62
BD_16_60	112.53	13.12	34.31	1.98	43.48	94.29
BL_16_120	103.71	4.25	24.78	1.81	31.16	86.19
BP_16_60	101.20	1.73	29.19	1.47	6.52	70.00

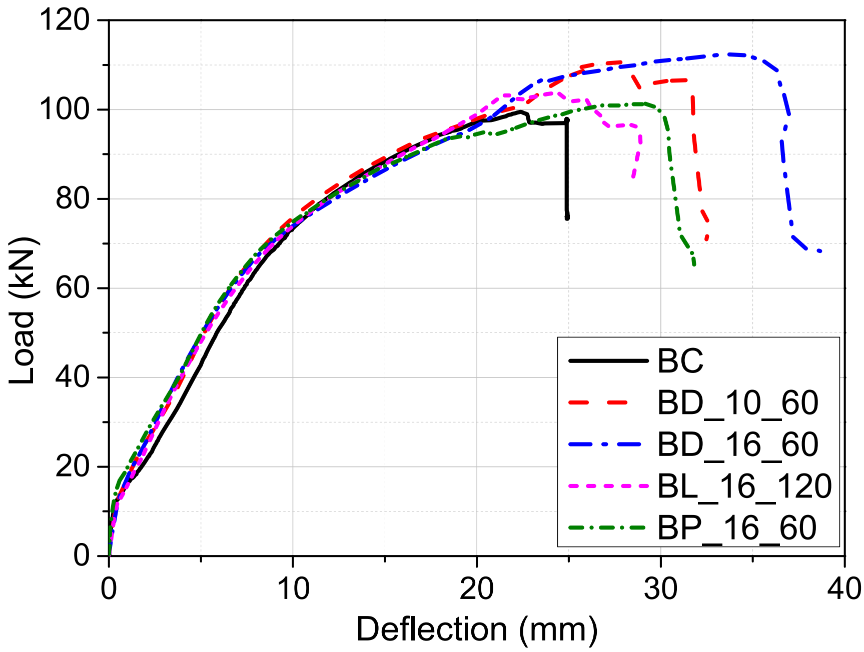

Figure 5. Load-deflection curves

3.1 Control specimen BC

The control specimen BC strengthened with BFRP sheets without anchorage at the beam soffit failed by intermediate crack (IC) debonding, as shown in Figure 6. This beam also failed at the lowest ultimate load of 99.48 kN and the smallest mid-span deflection of 22.38 mm among the five tested beams. The major flexural crack first initiated at mid-span, then propagated toward the plate end. As all the beams were heavily reinforced with stirrups, the failure was classified as flexural cracking. The FRP debonding was induced by the major flexural crack at mid-span and then propagated toward the right plate end, which limited the utilization of the capacity of BFRP sheets. As shown in Figure 7, the maximum debonding strain of 1.38% was recorded by the strain gauge S2 of Specimen BC, which was equal to 30.47% of the rupture strain (2.1%) from the BFRP coupon tests [40]. It was found that S2 experienced larger strain than S1 before debonding for Specimen BC, which might be caused by the thicker layer of epoxy applied at S2 location.

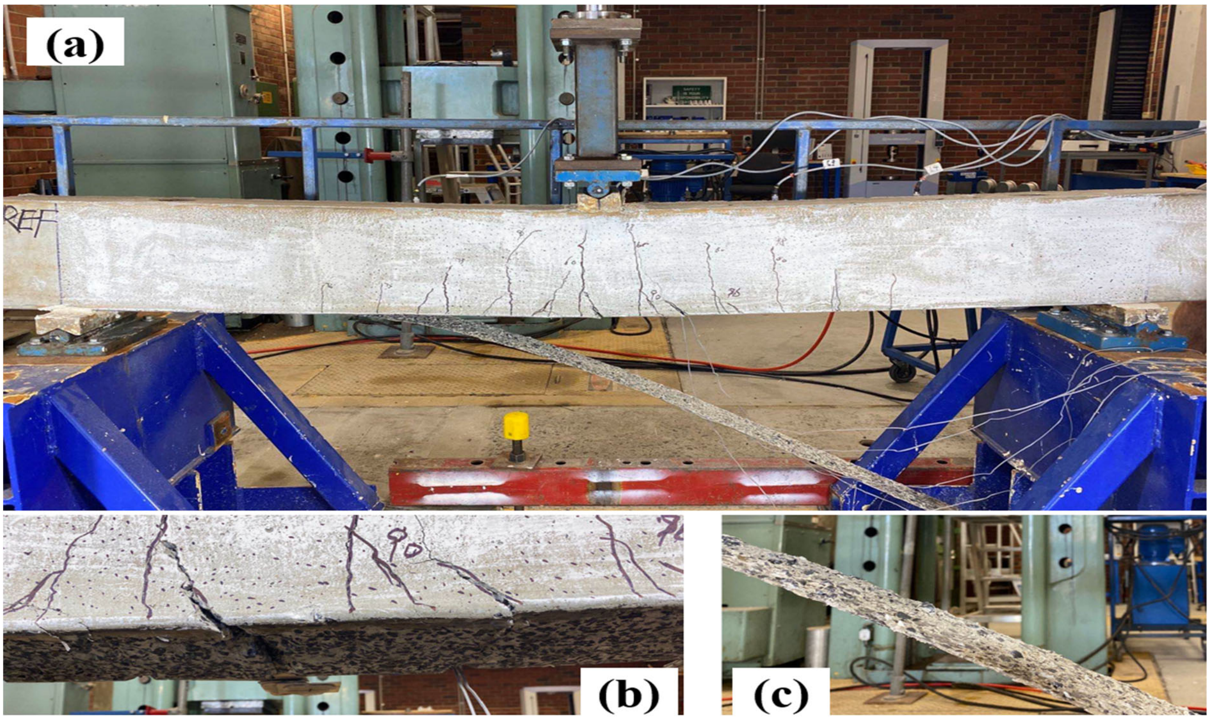

Figure 6. (a) Failure mode of control Specimen BC; (b) Concrete cracking after debonding; (c) Debonded BFRP sheets.

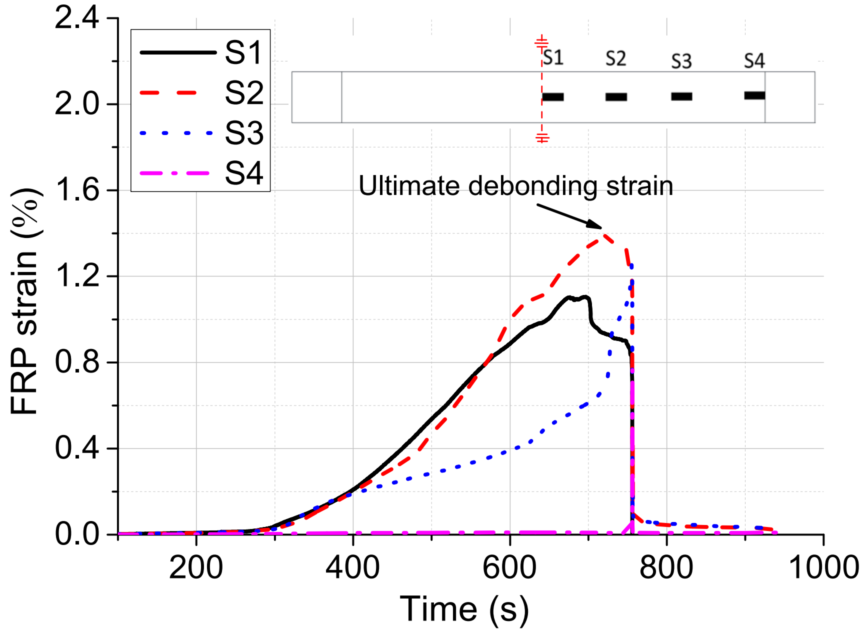

Figure 7. Strain-time history of control specimen BC

3.2 Specimen BD_10_60

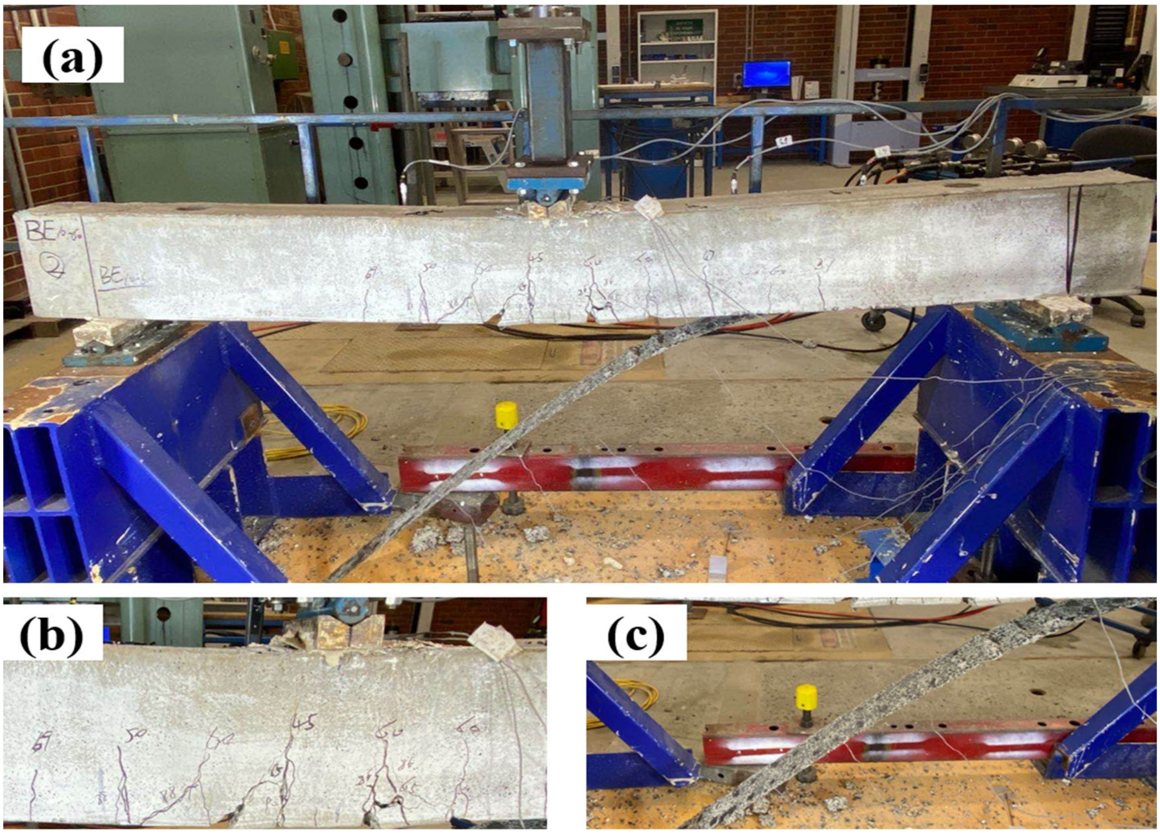

Figure 8. (a) Failure mode of Specimen BD_10_60; (b) Concrete cracking after debonding; (c) Detached BFRP sheets.

Specimen BD_10_60 had epoxy anchors with 10-mm-diameter at a spacing of 60 mm as described above. As shown in Figure 8, Specimen BD_10_60 experienced cracking with a thicker concrete layer as compared to the control specimen BC. During the debonding process, it was observed that the fracture of epoxy anchors started from mid-span and then propagated toward the supports. Due to the usage of anchorage, an ultimate applied load of 110.47 kN with a mid-span deflection of 27.79 mm was recorded. As shown in Figure 5, Specimen BD_10_60 had a similar initial stiffness as the control specimen BC with a similar load-deflection curve prior to the ultimate stage of Specimen BC (i.e., 99.48 kN). The anchorage configuration BD_10_60 exhibited higher ductility than the control specimen owing to the improved deflection at mid-span, indicating that the epoxy anchors provided additional ductility. Compared with Specimen BC, it was found that the ultimate load and the deformation of Specimen BD_10_60 increased by 11.05% and 24.17%, respectively. The improved load-carrying capability and ductility were due to the enhanced interfacial bonding between FRP and concrete, which was demonstrated by the improved ultimate debonding strain. As detailed in Figure 9, the peak debonding strain of 1.99% was recorded for S1, indicating that the enhanced strain capacity of FRP by 36.99% was achieved by using the epoxy anchors. Therefore, the epoxy anchor was effective in enhancing overall behaviour of the beam as the debonding strain greatly increased.

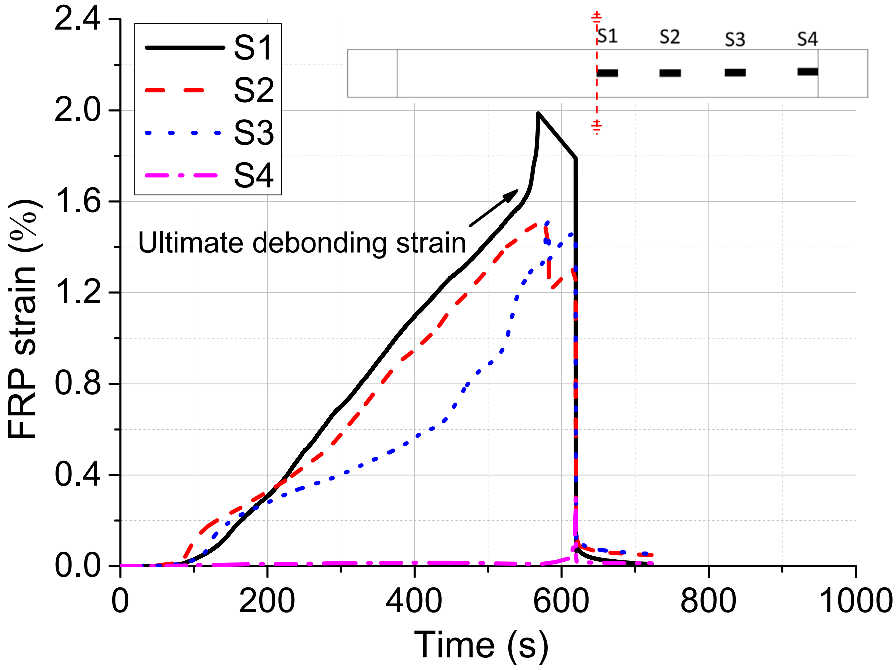

Figure 9. Strain-time history of Specimen BD_10_60

3.3 Specimen BD_16_60

Specimen BD_16_60 was prepared to exam the effect of anchor diameter on the flexural capacity. As shown in Figure 10, BD_16_60 experienced cracking with a thicker concrete layer due to the obvious flexural cracks as well as the pull-out of epoxy anchor. Specimen BD_16_60 experienced the rupture and pull-out of epoxy anchors as shown in Figure 10 (c), which initiated from the mid-span and then propagated toward the supports. Specimen BD_16_60 also experienced concrete compressive damage at the vicinity of the loading plate. As shown in Figure 5, the ultimate applied load of 112.53 kN and the corresponding deflection of 34.31 mm were recorded, which indicated a gain of 13.12% in flexural strength over the control specimen BC. An increase of 53.31% over the control specimen in the mid-span deflection was obtained by using 16-mm-diameter epoxy anchors, indicating that the beam ductility was remarkably affected by the anchor diameter. The enhancement in bending deflection is due to the efficient utilization of the FRP composite, as shown in Figure 11. The strain utilization (i.e., the ratio of debonding strain to ultimate strain) increased by 43.48% as compared to Specimen BC. The increment of anchor diameter from 10 mm to 16 mm enhanced the ultimate load-carrying capacity and improved the ultimate debonding strain, indicating that the increased anchorage size is beneficial to the enhancement of interfacial bond. The epoxy anchors with larger diameter (16 mm) were much more effective than the smaller one (10 mm) since the FRP strain along the beam was not uniform. Using larger-diameter anchors also changed the failure mode of epoxy anchors from fracture of 10-mm anchors to pull out of 16-mm anchors.

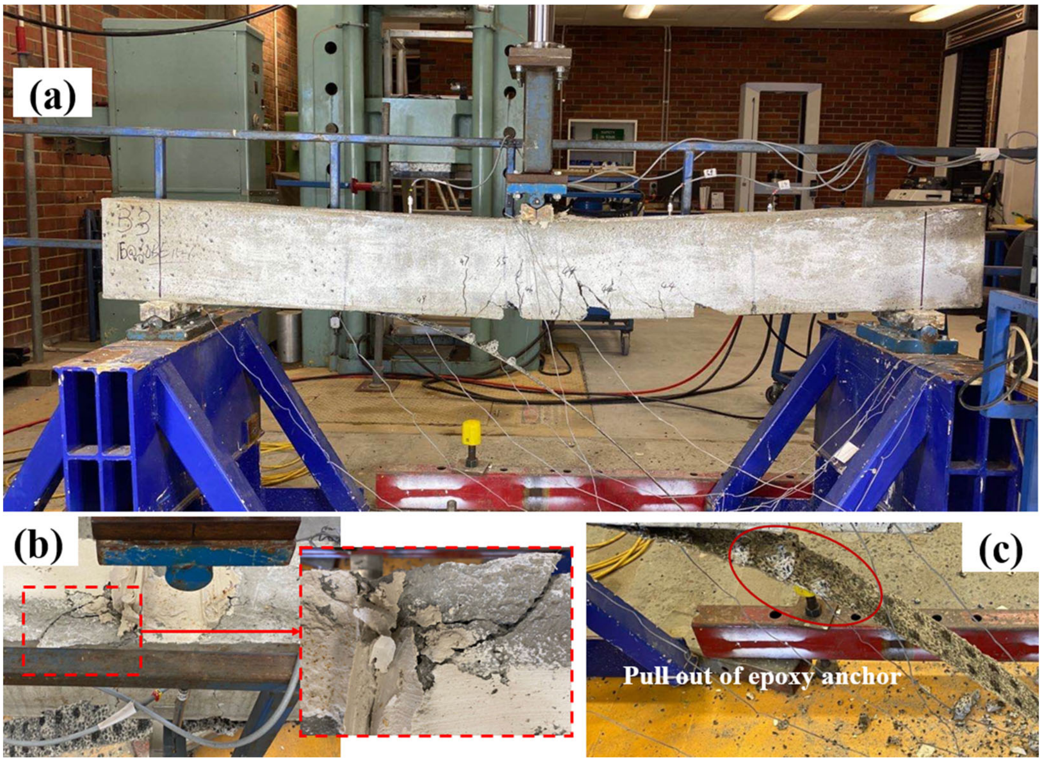

Figure 10. (a) Failure mode of Specimen BD_16_60; (b) Concrete compressive failure; (c) Debonded BFRP sheets.

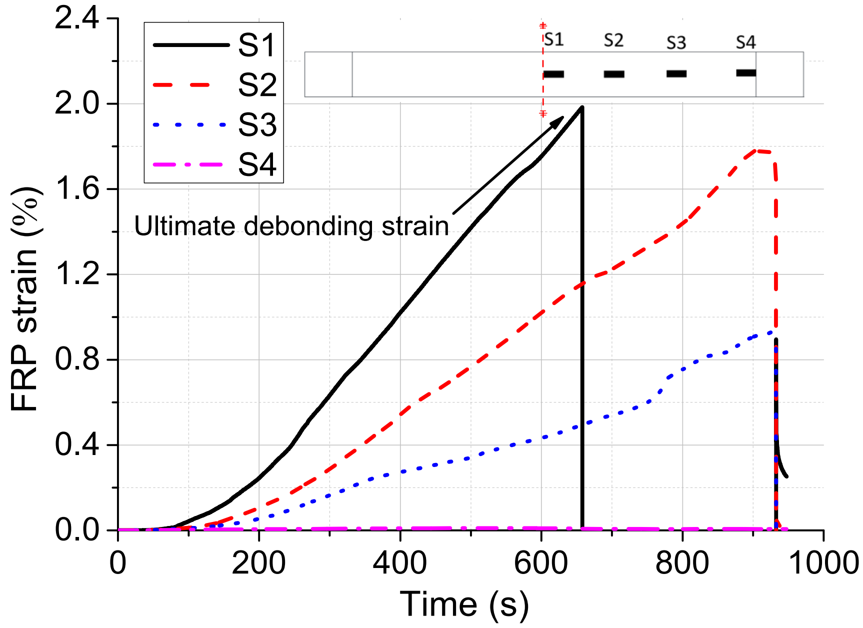

Figure 11. Strain-time history of Specimen BD_16_60

3.4 Specimen BL_16_120

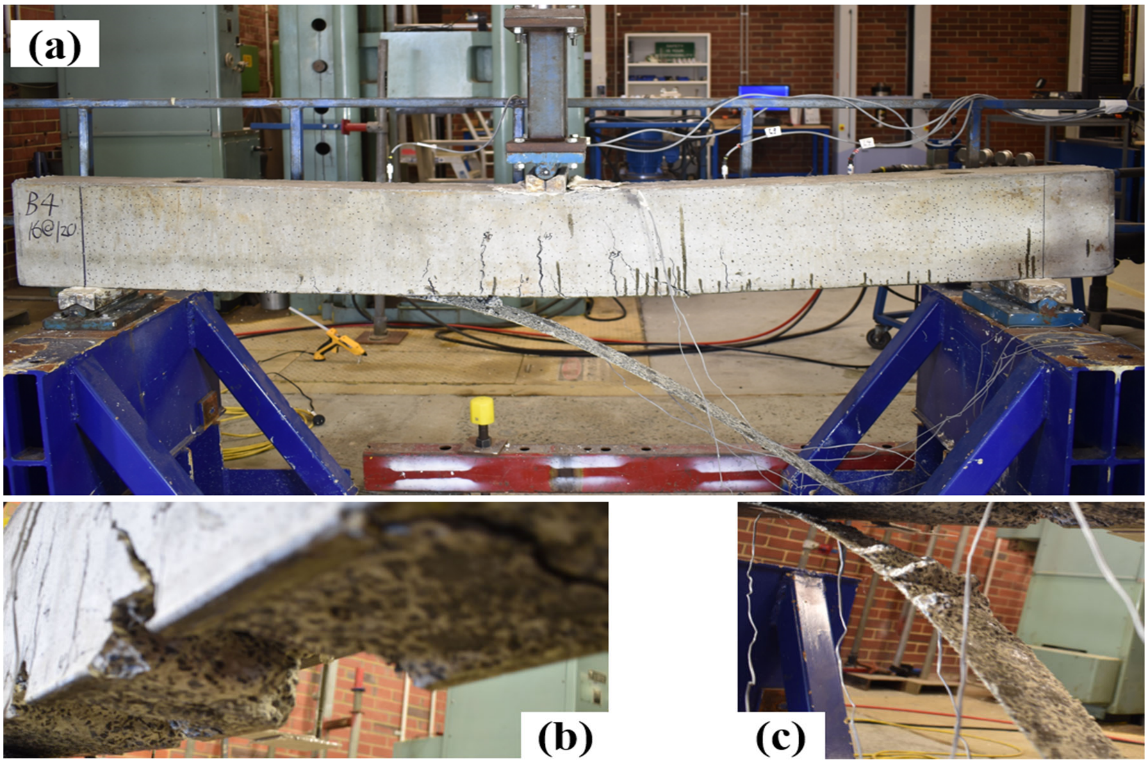

Figure 12. (a) Failure mode of Specimen BL_16_120; (b) Concrete cracking after debonding; (c) Debonded BFRP sheets.

Specimen BL_16_120 was used to examine the effect of spacing of epoxy anchor on the overall anchorage efficiency, as shown in Figure 12. As the effective bond length was found to be approximately 110 mm [36], the bond length of 120 mm is greater than the effective bond length, and the test was deliberately used to examine the influence of anchorage beyond the effective bond length. The ultimate applied load of 103.71 kN and the corresponding deflection of 24.78 mm were measured, which indicated a flexural strength gain of 4.25% over the control specimen BC. An increment of 10.72% over the control specimen in the mid-span deflection was obtained by using 16-mm-diameter epoxy anchors. The larger mid-span deflection is due to the efficient utilization of the FRP material, as shown in Figure 13. The strain utilization (i.e., the ratio of debonding strain to ultimate strain) increased by 31.16% over the control specimen. When the spacing between anchors increased from 60 mm to 120 mm (i.e., from BD_16_60 to BL_16_120), the load-carrying capacity of BL_16_120 showed a reduction from 112.53 kN to 103.71 kN. Additionally, the corresponding mid-span deflection (i.e., 24.78 mm) and the effective utilization of FRP material (i.e., 86.19%) have been significantly reduced with the increase of the anchor spacing, indicating that the increased anchorage spacing over the effective bond length cannot ensure the continuity of loading path.

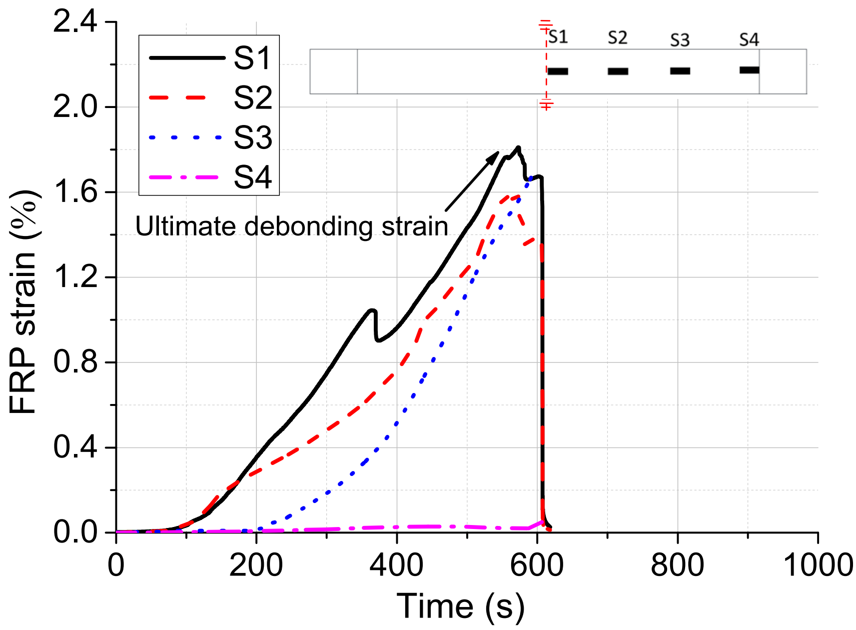

Figure 13. Strain-time history of Specimen BL_16_120

3.5 Specimen BP_16_60

To evaluate the influence of anchor coverage on the strengthening performance, Specimen BP_16_60 was prepared with 16-mm-diameter and 120-mm-spacing, but only in the mid sections of the FRP sheet as illustrated in Figure 14. The ultimate applied load of 101.20 kN and the corresponding deflection of 29.19 mm were recorded for this specimen, which indicated a flexural strength gain of 1.73% and an enhancement of 30.42% in the mid-span deflection over the control specimen. The enhancement in mid-span deflection is due to more efficient utilization of the FRP material, as shown in Figure 15. The strain utilization increased by 6.52% over the control specimen. However, as compared to Specimen BD_16_60, the partial anchorage showed a significant reduction in load-carrying capacity (i.e., 101.20 kN), mid-span deflection (i.e., 29.19 mm) and utilization of FRP material (i.e., 70%), indicating that partial anchorage was only effective for local interfacial bond. This can also be verified by the local failure of concrete with epoxy anchors, as shown in Figure 14 (b). Due to the partial coverage of epoxy anchors, the strain distribution at different locations was not uniform, and the destruction of concrete substrate was different at different locations. The concrete with anchorage experienced severer damage due to the peeling of thicker layer of concrete, as compared to the unanchored area. In addition, compared to partial anchorage, the loose anchorage case (i.e., Specimen BL_16_120) with an increase in the anchorage area improved the effective strain utilization as well as the deformation capacity.

Figure 14. (a) Failure mode of Specimen BP_16_60; (b) Concrete cracking after debonding; (c) Debonded BFRP sheets.

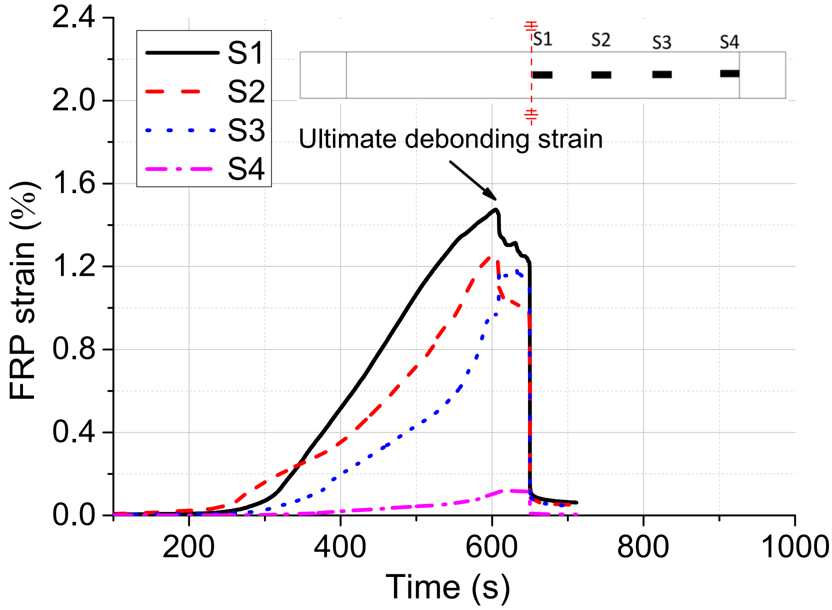

Figure 15. Strain-time history of Specimen BP_16_60

4. Comparisons and discussions

It was observed that all the specimens experienced flexural failure and IC debonding. The IC debonding failure in control beam occurred at the concrete layer, and the specimens with anchorage not only suffered the failure of concrete cover layer but also the rupture of epoxy anchors. Due to the interlocking action, the interfacial shear resistance was improved by using the epoxy anchors, which can be demonstrated by the increased load-carrying capacity. Additionally, the presence of epoxy anchors hardly changed the cracking and yielding stages of the strengthened specimens by experiencing similar load-deflection response, indicating the application of epoxy anchor had barely changed the overall stiffness of the beam. However, the ultimate stage of the anchored beams was prolonged over the control beam because of the strain hardening during the facture of the epoxy anchor, indicating that epoxy resin with high strain capacity would be beneficial to the improvement of the overall ductility of the strengthened beams.

To quantify the contribution of the epoxy anchors, strain gauges were mounted to the FRP sheet on beam soffit. Based on the strain-time curves, it was observed that different anchor configurations resulted in different strengthening efficiency. As the anchor size increased from 10 mm to 16 mm with the same anchorage spacing of 60 mm (i.e., BD_10_60 and BD_16_60), the strain utilization (i.e., the ratio of debonding strain to ultimate strain) increased remarkably from 1.63% to 1.98%, and larger deflection was experienced before the final detachment of BFRP sheets, indicating the large-size anchorage can provide better bond and hence the ductility of the beam. As the increase of anchorage spacing from 60 mm to 120 mm with the same anchor diameter of 60 mm (i.e., BD_16_60 and BL_16_120), the ultimate load-carrying capacity reduced from 112.53 kN to 103.71 kN, and the deflection decreased from 34.31 mm to 24.78 mm, indicating dense anchorage configuration can enhance flexural capacity and ductility. Furthermore, an increment in the anchorage area can improve the strain utilization and ductility by comparing with Specimen BL_16_120 and BP_16_60.

5. Analytical investigation

In general, the typical load-deflection behaviour of FRP-strengthened RC beams consists of three stages: (1) cracking stage; (2) yielding stage; and (3) ultimate stage, as shown in Figure 16. Semi-empirical models are proposed in this section based on conventional theories to estimate the flexural behaviour of the beams regarding the strength and the deformation at the cracking, yielding, and ultimate stages. The following assumptions are made to evaluate the flexural behaviour: (a) a plane beam cross-section remains plane after loading before yielding, which is based on Bernoulli beam theory; (b) the tensile strength of concrete is neglected since concrete tensile strength is much lower than compressive strength; and (c) the popularly used constitutive models of concrete [41], steel [42], and FRP, summarized in Table 2.

Table 2. Material constitutive models [41, 42]

	Concrete	Steel	FRP
Constitutive law	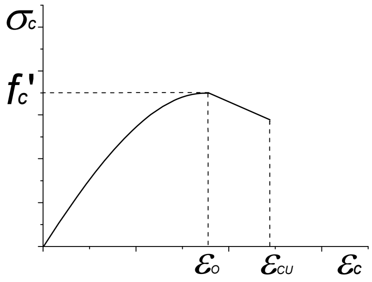	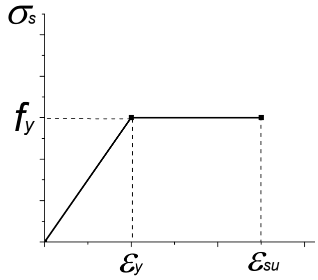	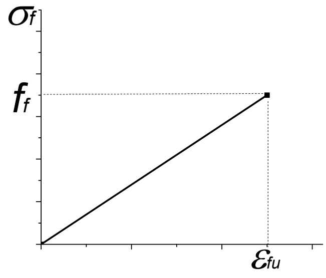
Formulae	$\sigma_c = f_c'\left(\frac{2\varepsilon_c}{\varepsilon_o} - \left(\frac{\varepsilon_c}{\varepsilon_o}\right)^2\right) \quad 0 \le \varepsilon_c \le \varepsilon_o$ $\sigma_c = f_c'\left[1 - 0.15\left(\frac{\varepsilon_c - \varepsilon_o}{\varepsilon_{cu} - \varepsilon_o}\right)\right] \quad \varepsilon_o < \varepsilon_c$	$\sigma_s = \varepsilon_s E_s \quad \varepsilon_s \le \varepsilon_y$ $\sigma_s = f_y \quad \varepsilon_s > \varepsilon_y$	$\sigma_f = \varepsilon_f E_f \quad \varepsilon_f \le \varepsilon_{fu}$

Note: f_c', f_y, and f_f refer to the concrete compressive strength, the yielding strength of reinforcement rebar, the ultimate tensile strength of BFRP, respectively; σ_c, σ_s, and σ_f represent the concrete compressive strength, the tensile strength of steel reinforcement, and the tensile strength of BFRP at different loading stages, respectively; ε_c, ε_s, ε_f refer to the concrete strain, steel reinforcement strain, and BFRP strain at different loading levels, respectively; ε_o, ε_{cu}, ε_y, ε_{su}, and ε_{fu} represent the peak strain of concrete, the ultimate strain of concrete, the yielding strain of steel reinforcement, the rupture strain of steel reinforcement, and the rupture strain of BFRP sheet, respectively; and E_s and E_f refer to the elastic modulus of steel reinforcement and BFRP sheet.

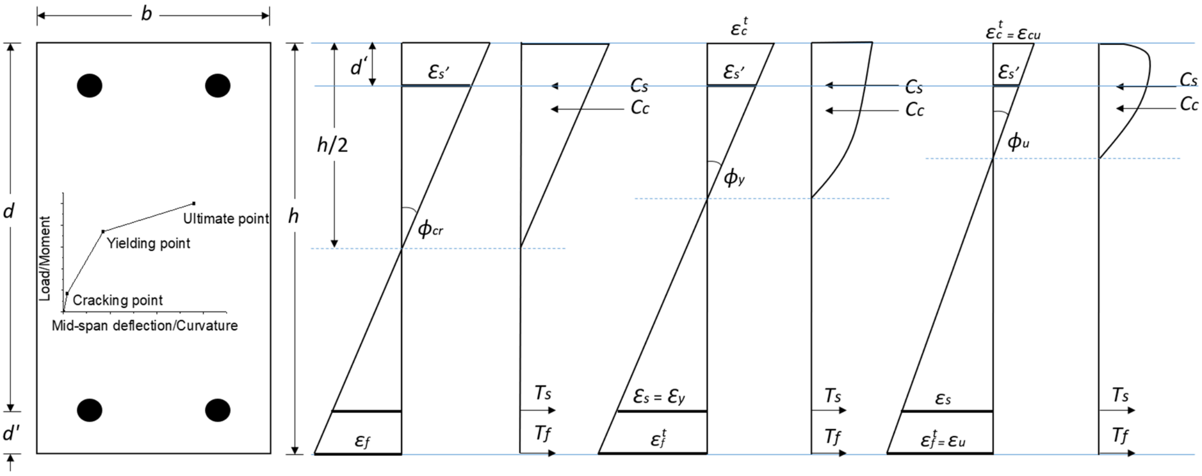

(a) Cracking stage (b) Yielding stage (c) Ultimate stage

Figure 16. Strain diagram and stress blocks at three stages (cracking, yielding, and ultimate stage)

5.1 Determination of cracking moment

Figure 17. The definition of cracking point for all specimens

Cracking moment denoted as (M_{cr}) is defined as the moment causing the cracking of concrete. The definition of cracking point can be seen in Figure 17. Based on conventional theories, the cracking moment (M_{cr}), the load at the cracking moment (P_{cr}), and the mid-span deflection (δ_{cr}) at cracking stage can be obtained by the following formulae [43, 44]:

$$M_{cr} = \frac{f_r I_g}{y_t} \quad (1)$$

$$I_g = \frac{bh^3}{12} + 2nA_s\left(\frac{h}{2} - d^{'}\right)^2 \quad (2)$$

$$P_{cr} = \frac{2M_{cr}}{L_d} \quad (3)$$

$$\delta_{cr} = \frac{M_{cr}}{6E_c I_g}\left(\frac{3L_d^{\ 2}}{4} - \frac{L_d}{2}\right) \quad (4)$$

in which f_r refers to the concrete modulus of rupture, which can be expressed as $0.62\sqrt{f_c^{'}}$ based on the recommendation by ACI 318-11 [45], y_t refers to the distance from the gravity centre of beam to the extreme fiber of the tension side, I_g refers to the moment of the beam, A_s represents area of compression and tension reinforcement, d' refers to the distance from bottom surface to center of tension reinforcement bars, n refers to the ratio between elastic modulus of steel (E_s) and concrete (E_c), L_d is the effective span of beam, M_{cr} refers to the cracking moment, and P_{cr} is the load at the cracking moment.

5.2 Determination of yielding moment

As the applied load increased, the longitudinal reinforcement and FRP carried the tensile force. By assuming that the yield of steel occurs before flexural failure, the conventional section analysis similar to that for normal RC members can be adopted. The definition of yielding point can be found in Figure 18. Tension steel stress f_s is equal to the yield stress f_y. At the yielding stage, the flexural strength M_y can be obtained using Equation (5), which is based on the force equilibrium in Equation (6) of the cross section [43].

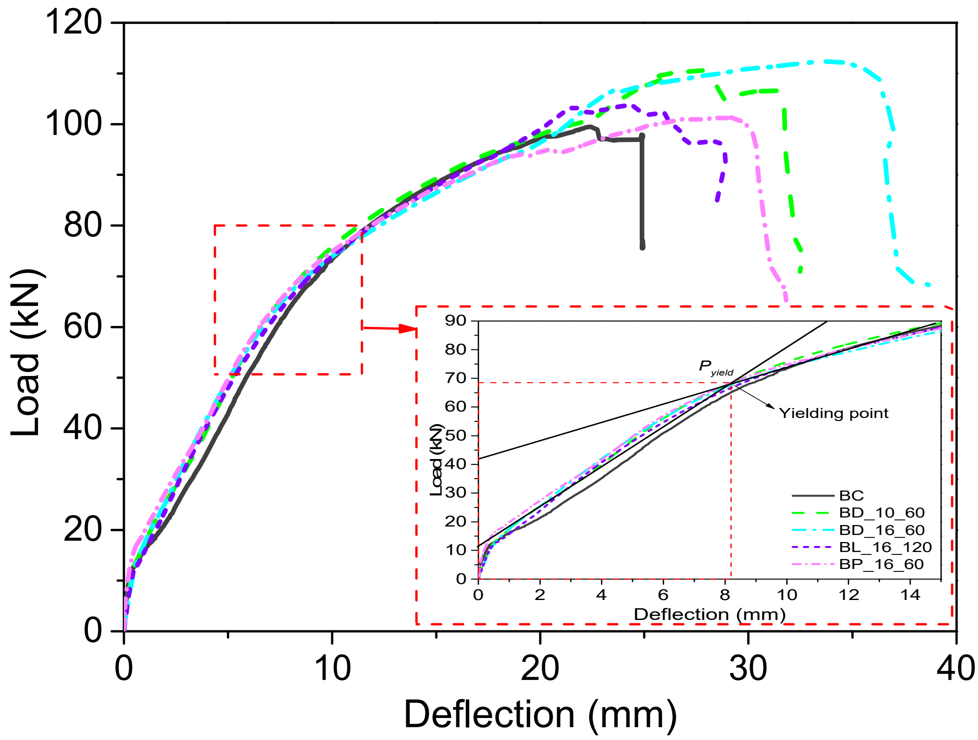

Figure 18. The definition of yielding point for all specimens

$$M_y = f_y A_s \left(d - k_1 c_y\right) + f_f A_f \left(h - k_1 c_y\right) + f_s^{'} A_s^{'} \left(k_1 c_y - d^{'}\right) \tag{5}$$

$$k_2 f_c^{'} b c_y + f_s^{'} A_s^{'} = f_y A_s + f_f A_f \tag{6}$$

in which f_y is the yielding strength of reinforcement bars, $f_s{'}$ is the compressive strength of reinforcement bars, f_f is the tensile strength of BFRP sheet, A_f is area of BFRP sheets, d refers to the distance between the top concrete fiber and the centroid of the tension reinforcement bars, h is the depth of concrete beam, c_y represents the depth of the neutral axis, and k_1 and k_2 are the parameters which can be obtained from the modified Hognestad's concrete compressive model [41] as given in Equation (7) and (8).

$$k_1 = \left(\frac{1}{3} - \frac{\varepsilon_c}{12\varepsilon_o}\right) \Big/ \left(1 - \frac{\varepsilon_c}{3\varepsilon_o}\right), \quad 0 \le \varepsilon_c \le \varepsilon_o \tag{7}$$

$$k_1 = \frac{3\varepsilon_c - \varepsilon_o}{3\varepsilon_c} - \frac{0.075}{\varepsilon_{cu} - \varepsilon_o}\left(\varepsilon_c + \frac{\varepsilon_o^{\ 2}}{\varepsilon_c} - 2\varepsilon_o\right), \quad \varepsilon_o \le \varepsilon_c \le \varepsilon_{cu} \tag{8}$$

in which ε_c refers to the concrete compressive strain, ε_o represents the compressive strain at maximum stress, which is obtained according to the recommendation of ACI 440.2R-02 [43] and the ultimate compressive strain ε_{cu} is 0.0033. According to similar triangle of strain profile, the strain in the BFRP sheets and that in compression reinforcement bar can be obtained by using Equation (9) and (10) as follows.

$$\varepsilon_f = \frac{h-c_y}{d-c_y}\varepsilon_y - \varepsilon_o \tag{9}$$

$$\varepsilon_s^{'} = \frac{c_y-d^{'}}{d-c_y}\varepsilon_y \tag{10}$$

in which ε_f is the tensile strain of BFRP sheet and ε_y is the yielding strain of reinforcement bar. The depth of the neutral axis c_y can be obtained using Equation (6). The parameter k_2 in Equation (6) can be obtained by using Equation (12), based on the force equilibrium in Equation (11):

$$k_2 f_c^{'} b c_y = \frac{\int_0^{\varepsilon_c} f_c \, d\varepsilon_c}{\varepsilon_c f_c{'}} \tag{11}$$

$$k_2 = \frac{\varepsilon_c}{\varepsilon_o} - \frac{\varepsilon_c^{\;2}}{3\varepsilon_o^{\;2}}, \quad 0 \le \varepsilon_c \le \varepsilon_o \tag{12}$$

$$k_2 = \frac{3\varepsilon_c - \varepsilon_o}{3\varepsilon_c} - \frac{0.075}{\varepsilon_{cu} - \varepsilon_o}\left(\varepsilon_c + \frac{\varepsilon_o^{\;2}}{\varepsilon_c} - 2\varepsilon_o\right), \quad \varepsilon_o \le \varepsilon_c \le \varepsilon_{cu} \tag{13}$$

The beam curvature can be used to determine the mid-span deflection at yielding stage. The corresponding curvature can be obtained from the slope of the strain diagram for the beam section, as shown in Figure 16. The curvature (ϕ_y) at the yielding stage can be expressed as follows:

$$\phi_y = \frac{\varepsilon_y}{d-c} \tag{14}$$

5.3 Determination of ultimate moment

The ultimate moment of beams mainly depends on its final failure mode. In general, the IC debonding was observed for all the beams in this study. Numerous studies [43, 46-54] have been conducted to estimate the FRP strain at the occurrence of IC debonding failure, and the corresponding analytical models for debonding strain have been proposed, as given in Table 3. A total of 12 IC debonding strain models have been used for comparison. By comparing the predicted results, the model proposed by Elsanadedy et al. [54] gave the most accurate estimations with the ratio of predicted and test obtained mean of 1.10 and CoV of 0.89.

Table 3. Models for IC debonding strain [55]

Model	Equations	Prediction		
		Mean*	CoV	Case
ACI440.2R-08 [43]	$\varepsilon_{f,u}=0.41\sqrt{f'_c/(E_f t_f)}\le 0.9\varepsilon_{fu}$	1.17	0.13	with anchor
		0.94	/	no anchor
CNR [46]	$\varepsilon_{f,u}=0.373\sqrt{\beta_b\sqrt{f_{ct}f'_c}/(E_f t_f)}$	1.95	0.13	with anchor
	$\beta_b=\sqrt{(2-b_f/b)/(1+b_f/b)}$	1.56	/	no anchor
CIDAR [47]	$\varepsilon_{f,u}=0.379\beta_b\sqrt{\sqrt{f'_c}/(E_f t_f)}$	1.62	0.13	with anchor
	$\beta_b=\sqrt{(2-b_f/b)/(1+b_f/b)}$	1.30	/	no anchor
TR55 [48]	$\varepsilon_{f,u}=0.5\beta_b\sqrt{f_{ct}/(E_f t_f)}$	3.72	0.13	with anchor
	$\beta_b=1.06\sqrt{(2-b_f/b)/(1+b_f/400)}$	2.98	/	no anchor
JSCE [49]	$\varepsilon_{f,u}=\sqrt{2G_f/(E_f t_f)}$	1.92	0.13	with anchor
		1.54	/	no anchor
Teng et al. [50]	$\varepsilon_{f,u}=0.48\beta_b\beta_L\sqrt{\sqrt{f'_c}/(E_f t_f)}$	2.94	0.13	with anchor
	$\beta_b=\sqrt{(2-b_f/b)/(1+b_f/b)}$	2.36	/	no anchor
Lu et al. [51]	$\varepsilon_{f,u}=1.5\beta_b f_{ct}\left[\left(0.503/\sqrt{E_f t_f}\right)-\left(0.0866/L_d\right)\right]$	1.45	0.13	with anchor
	$\beta_b=\sqrt{(2-b_f/b)/(1+b_f/b)}$	1.16	/	no anchor
Said and Wu [52]	$\varepsilon_{f,u}=0.23\left(f'_c\right)^{0.2}/\left(n_f E_f t_f\right)^{0.35}$	1.34	0.13	with anchor
		1.10	/	no anchor
Wu and Niu [53]	$\varepsilon_{f,u}=\sqrt{2G_f/(E_f t_f)}\quad G_f=0.644f_c^{0.19}$	2.03	0.13	with anchor
		1.63	/	no anchor
Elsanadedy et al. [54]	$\varepsilon_{f,u}=\frac{\beta_b}{1.55}\left(\frac{\varepsilon_y}{E_f t_f}\right)^{0.4}\left(6.5+\frac{E_f t_f}{135000}\right)\rho_s^{0.05}f'^{\,0.1}_c$	1.10	0.13	with anchor
	$\beta_b=\left[(2-b_f/b)/(1+b_f/b)\right]^{0.1}$	0.89	/	no anchor

Note: Mean refers to the average ratio between predicted and experimental results.*

The flexural capacity M_u can be obtained using Equation (15), based on the force equilibrium in Equation (16) of the cross section. The parameters k_1 and k_2 can be obtained from the modified Hognestad's model [41].

$$M_u = f_y A_s \left(d - k_1 c_u\right) + f_f A_f \left(h - k_1 c_u\right) + f_s^{'} A_s^{'} \left(k_1 c_u - d^{'}\right) \tag{15}$$

$$k_2 f_c^{'} b c_u + f_s^{'} A_s^{'} = f_y A_s + f_f A_f \tag{16}$$

As the failure mode is FRP debonding, the ultimate debonding strain can be predicted by using Equation (17) as proposed by Elsanadedy et al. [54]. According to the strain compatibility, the strain of steel and concrete correlated with the FRP ultimate debonding strain are expressed in Equation (18) and (19):

$$\varepsilon_{f,u} = \frac{\beta_b}{1.55}\left(\frac{\varepsilon_y}{E_f t_f}\right)^{0.4}\left(6.5 + \frac{E_f t_f}{135000}\right)\rho_s^{0.05} {f_c^{'}}^{0.1} \tag{17}$$

$$\varepsilon_s^{'} = \frac{c_u - d^{'}}{h - c_u}\varepsilon_{f,u} \tag{18}$$

$$\varepsilon_c = \frac{c_u}{h - c_u}\varepsilon_{f,u} \tag{19}$$

$$\phi_u = \frac{\varepsilon_{f,u}}{h - c_u} \tag{20}$$

To achieve more accurate predictions, the ultimate debonding strain obtained by Equation (17) needs a calibration factor (i.e., the mean value of the predicated ultimate debonding strain given in Table 3 to consider the contribution by the epoxy anchors). The calibration factor of 1.1 was obtained based on the testing data. The application of epoxy anchors hardly changed the beam stiffness but improved the ultimate debonding strain of FRP sheets. Therefore, the ultimate moment varied with different anchorage configurations. The obtained curvature will be involved to obtain the mid-span deflection in the following section.

5.4 Determination of mid-span deflection

The result for curvature at each stage can be obtained by implementing the integration of the moment of curvature [56]. The deflection at mid-span can be calculated by integrating the function of curvature distribution along the beam axis as follows:

$$\delta\left(x\right)=\iint\phi\left(x\right)dx \tag{21}$$

in which $\delta(x)$ and $\phi(x)$ refer to the deflection and curvature along the beam axis (x). As proposed by Rasheed et al. [57], the simplified analytical equations can be expressed as follows:

$$\delta_{midspan}=\int_{0}^{L_g}x\phi_{cr}\left(x\right)dx+\int_{L_g}^{L_y}x\phi_{y}\left(x\right)dx+\int_{L_y}^{L/2}x\phi_{u}\left(x\right)dx \tag{22}$$

in which L_g refers to the uncracked region, L_y represents the post cracked region, and L is the span of the beam. The experimental and analytical results for the loading capacity and the corresponding mid-span deflection for BC and BD_16_60 are summarized in Table 4. It is found that the proposed analytical approach can give good predictions of the load-carrying capacity in general, as shown in Figure 19. The ultimate loads derived from the proposed analytical model matched well with the test results, indicating the debonding strain can be well predicted by using the Elsanadedy et al. [54] equation with the calibration factor. It should be noted that the predicted mid-span deflection shows discrepancy in the post-yielding stage and the ultimate deflection is underestimated for BD_16_60. It might be because the concrete cracking and reinforcement slippage in the test are not considered in the analytical model.

Table 4. Experimental and analytical results

ID	Cracking stage				Yielding stage				Ultimate stage			
	P_{cr} (kN) (Exp.)	P_{cr} (kN) (Pre.)	δ_{cr} (mm) (Exp.)	δ_{cr} (mm) (Pre.)	P_y (kN) (Exp.)	P_y (kN) (Pre.)	δ_y (mm) (Exp.)	δ_y (mm) (Pre.)	P_u (kN) (Exp.)	P_u (kN) (Pre.)	δ_u (mm) (Exp.)	δ_u (mm) (Pre.)
BC	11.96	12.06	0.30	0.31	72.10	65.12	8.21	6.35	99.48	95.0	22.38	20.0
BD_16_60	12.12	12.06	0.43	0.31	73.78	65.12	8.43	6.35	112.53	113.0	34.31	33.0

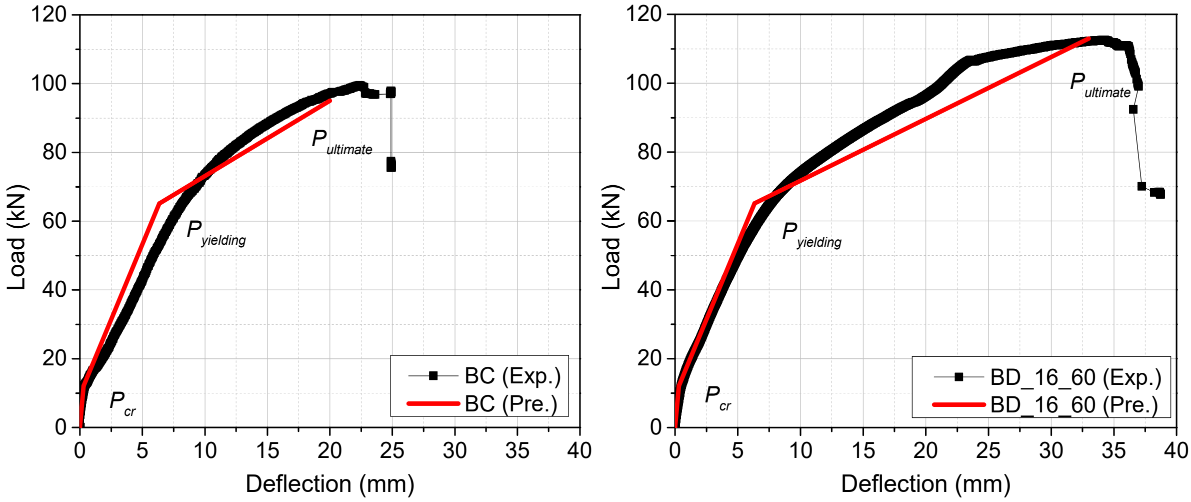

Figure 19. Comparison of testing and predicted load-deflection responses (L) BC; (R) BD_16_60

6. Conclusions

The effectiveness of applying new epoxy anchors in mitigating IC debonding for BFRP-retrofitted RC beams was examined in this study. Five specimens were prepared with different anchorage configurations of new epoxy anchors. The influences of anchorage diameter, anchorage spacing and anchorage area on the structural performance were examined and the most effective anchorage configuration was identified. The experimental results clearly demonstrated that increasing the anchor size, anchorage density and area over the FRP sheet all enhance the performance of the FRP strengthened RC beams considering the loading and deformation capability. Based on the experimental and analytical results presented in the paper, the following particular conclusion can be drawn:

1. Applying epoxy anchors with 16-mm-diameter and 60-mm-spacing (i.e., Specimen BD_16_60) enhanced the load-carrying capacity by 13.12% and the deflection by 53.31% (ductility) as compared to the one without anchor (i.e., Specimen BC).
2. Applying epoxy anchors with 16-mm-diameter and 60-mm-spacing (i.e., Specimen BD_16_60) achieved the best interfacial bonding resistance among the tested beams due to the enhanced ultimate debonding strain by 47.79% (i.e., from 1.36% to 2.01%) as compared to Specimen BC.

3. The analytical approach was able to predict the load-carrying capacity of RC beams reinforced with BFRP sheets with or without epoxy anchors.

Acknowledgements

The authors are grateful for financial support from Australian Research Council (Grant No. LP150100259) to carry out this study. Thanks are also given to Mr. Kevin Reilly and Tuan Ngo for their assistance during the test.

References

[1] J. Teng, J. Yao, Plate end debonding in FRP-plated RC beams—II: Strength model, Eng. Struct. 29(10) (2007) 2472-2486.
[2] J. Dong, Q. Wang, Z. Guan, Structural behaviour of RC beams with external flexural and flexural–shear strengthening by FRP sheets, Compos. B. Eng. 44(1) (2013) 604-612.
[3] B.N. Tehrani, D. Mostofinejad, S.M. Hosseini, Experimental and analytical study on flexural strengthening of RC beams via prestressed EBROG CFRP plates, Eng. Struct. 197 (2019) 109395.
[4] C. Yuan, W. Chen, T.M. Pham, H. Li, H. Hao, Finite element modelling of dynamic bonding behaviours between fibre reinforced polymer sheet and concrete, Construction and Building Materials 255 (2020) 118939.
[5] C. Yuan, W. Chen, T.M. Pham, H. Hao, J. Cui, Y. Shi, Influence of Concrete Strength on Dynamic Interfacial Fracture Behaviour between Fibre Reinforced Polymer Sheets and Concrete, Eng. Struct. (2020) 106934.
[6] C. Yuan, W. Chen, T.M. Pham, L. Chen, J. Cui, Y. Shi, H. Hao, Effect of aggregate size on the dynamic interfacial bond behaviour between basalt fiber reinforced polymer sheets and concrete, Constr. Build. Mater. 227 (2019a) 116584.
[7] C.A. Coronado, M.M. Lopez, Damage approach for the prediction of debonding failure on concrete elements strengthened with FRP, J. Compos. Constr. 11(4) (2007) 391-400.
[8] T.M. Pham, H. Hao, Behavior of fiber-reinforced polymer-strengthened reinforced concrete beams under static and impact loads, International Journal of Protective Structures 8(1) (2017) 3-24.
[9] Y. Jiangtao, W. Yichao, H. Kexu, Y. Kequan, X. Jianzhuang, The performance of near-surface mounted CFRP strengthened RC beam in fire, Fire Safety Journal 90 (2017) 86-94.
[10] J. Sim, C. Park, Characteristics of basalt fiber as a strengthening material for concrete structures, Compos. B. Eng. 36(6) (2005) 504-512.
[11] R. Kalfat, R. Al-Mahaidi, S.T. Smith, Anchorage devices used to improve the performance of reinforced concrete beams retrofitted with FRP composites: State-of-the-art review, J. Compos. Constr. 17(1) (2013) 14-33.
[12] H. Yuan, J. Teng, R. Seracino, Z. Wu, J. Yao, Full-range behavior of FRP-to-concrete bonded joints, Eng. Struct. 26(5) (2004) 553-565.
[13] H.A. Baky, U. Ebead, K. Neale, Nonlinear micromechanics-based bond–slip model for FRP/concrete interfaces, Eng. Struct. 39 (2012) 11-23.
[14] J. Xiao, J. Li, Q. Zha, Experimental study on bond behavior between FRP and concrete, Construction and building materials 18(10) (2004) 745-752.
[15] S.V. Grelle, L.H. Sneed, Review of anchorage systems for externally bonded FRP laminates, Int. J. Concr. Struct. M. 7(1) (2013) 17-33.

[16] J.W. Schmidt, A. Bennitz, B. Täljsten, P. Goltermann, H. Pedersen, Mechanical anchorage of FRP tendons–A literature review, Constr. Build. Mater. 32 (2012) 110-121.
[17] Y. Zhou, X. Chen, Z. Fan, L. Sui, D. Li, F. Xing, Bond behaviors of FRP-to-concrete interface under the control of a novel end-anchorage system, Compos. Struct. 168 (2017) 130-142.
[18] W. Chen, T.M. Pham, M. Elchalakani, H. Li, H. Hao, L. Chen, Experimental and Numerical Study of Basalt FRP Strip Strengthened RC Slabs under Impact Loads, International Journal of Structural Stability and Dynamics (2020).
[19] R. Al-Mahaidi, R. Kalfat, Investigation into CFRP laminate anchorage systems utilising bi-directional fabric wrap, Compos. Struct. 93(4) (2011) 1265-1274.
[20] B. Fu, X. Tang, L. Li, F. Liu, G. Lin, Inclined FRP U-jackets for enhancing structural performance of FRP-plated RC beams suffering from IC debonding, Compos. Struct. 200 (2018) 36-46.
[21] T.M. Pham, H. Hao, Impact behavior of FRP-strengthened RC beams without stirrups, J. Compos. Constr. 20(4) (2016) 04016011.
[22] W. Chen, T.M. Pham, H. Sichembe, L. Chen, H. Hao, Experimental study of flexural behaviour of RC beams strengthened by longitudinal and U-shaped basalt FRP sheet, Compos. B. Eng. 134 (2018) 114-126.
[23] J. Lee, M.M. Lopez, Characterization of FRP Uwrap anchors for externally bonded FRP-reinforced concrete elements: An experimental study, J. Compos. Constr. 20(4) (2016) 04016012.
[24] B. Fu, J.G. Teng, J.F. Chen, G.M. Chen, Y.C. Guo, Concrete Cover Separation in FRP-Plated RC Beams: Mitigation Using FRP U-Jackets, J. Compos. Constr. 21(2) (2016) 04016077.
[25] E. Del Rey Castillo, D. Dizhur, M. Griffith, J. Ingham, Strengthening RC structures using FRP spike anchors in combination with EBR systems, Compos. Struct. 209 (2019) 668-685.
[26] E. del Rey Castillo, R. Kanitkar, S.T. Smith, M.C. Griffith, J.M. Ingham, Design approach for FRP spike anchors in FRP-strengthened RC structures, Compos. Struct. 214 (2019) 23-33.
[27] S.T. Smith, J. Teng, FRP-strengthened RC beams. I: review of debonding strength models, Eng. Struct. 24(4) (2002) 385-395.
[28] H. Zhang, S.T. Smith, Influence of plate length and anchor position on FRP-to-concrete joints anchored with FRP anchors, Compos. Struct. 159 (2017) 615-624.
[29] H. Zhang, S.T. Smith, R.J. Gravina, Z. Wang, Modelling of FRP-concrete bonded interfaces containing FRP anchors, Constr. Build. Mater. 139 (2017) 394-402.
[30] A.J. Lamanna, L.C. Bank, D.T. Borowicz, Mechanically fastened FRP strengthening of large scale RC bridge T beams, Adv. Struct. Eng. 7(6) (2004) 525-538.
[31] J.H. Lee, M.M. Lopez, C.E. Bakis, Slip effects in reinforced concrete beams with mechanically fastened FRP strip, Cement. Concrete. Comp. 31(7) (2009) 496-504.
[32] J.A. Martin, A.J. Lamanna, Performance of mechanically fastened FRP strengthened concrete beams in flexure, J. Compos. Constr. 12(3) (2008) 257-265.
[33] R. Realfonzo, E. Martinelli, A. Napoli, B. Nunziata, Experimental investigation of the mechanical connection between FRP laminates and concrete, Compos. B. Eng. 45(1) (2013) 341-355.
[34] Y.-F. Wu, Y. Huang, Hybrid bonding of FRP to reinforced concrete structures, J. Compos. Constr. 12(3) (2008) 266-273.
[35] Y.-F. Wu, L. He, L. Bank, Bond-test protocol for plate-to-concrete interface involving all mechanisms, J. Compos. Constr. 20(1) (2015) 04015022.
[36] C. Yuan, W. Chen, T.M. Pham, H. Hao, L. Chen, M. Zhang, New epoxy anchor for better bonding between FRP sheets and concrete, Constr. Build. Mater. 248 (2020) 118628.
[37] C. Jiang, B. Wan, Y.-F. Wu, J. Omboko, Epoxy interlocking: A novel approach to enhance FRP-to-concrete bond behavior, Constr. Build. Mater. 193 (2018) 643-653.
[38] S.T. Smith, H. Zhang, Z. Wang, Influence of FRP anchors on the strength and ductility of FRP-strengthened RC slabs, Constr. Build. Mater. 49 (2013) 998-1012.

[39] C. ASTM, Standard test method for compressive strength of cylindrical concrete specimens, 2012.
[40] C. Yuan, W. Chen, T.M. Pham, H. Hao, J. Cui, Y. Shi, Strain rate effect on interfacial bond behaviour between BFRP sheets and steel fibre reinforced concrete, Compos. B. Eng. (2019) 107032.
[41] E. Hognestad, Study of combined bending and axial load in reinforced concrete members, University of Illinois at Urbana Champaign, College of Engineering, 1951.
[42] C. Eurocode, Design of steel structures-Part 1-1: General rules and rules for buildings, CEN, Brussels: European Committee for Standardization (2005).
[43] A. 440.2R-08, Guide for the design and construction of externally bonded FRP systems for strengthening concrete structures. ACI Committee 440, Farmington Hills, Michigan; 2008., (2008).
[44] T.T. Tran, T.M. Pham, H. Hao, Experimental and analytical investigation on flexural behaviour of ambient cured geopolymer concrete beams reinforced with steel fibers, Eng. Struct. 200 (2019) 109707.
[45] A.A. Standard, Building Code Requirements for Structural Concrete (ACI 318-11), American Concrete Institute, 2011.
[46] CNR, Guide for the design and construction of an externally bonded FRP system for strengthening existing structures, Italian National Research Council, Rome (2012).
[47] CIDAR, Design guideline for RC structures retrofitted with FRP and metal plates: Beams and slabs, 2006.
[48] S. Concrete Society, Design guidance for strengthening concrete structures using fibre composite materials Report of a Concrete Society committee, 2000.
[49] K. Maruyama, T. Ueda, JSCE recommendations for upgrading of concrete structures with use of continuous fiber sheets, FRP Composites in Civil Engineering. Proceedings of the International Conference on FRP composites in Civil EngineeringHong Kong Institution of Engineers, Hong Kong Institution of Steel Construction, 2001.
[50] J. Teng, S.T. Smith, J. Yao, J.F. Chen, Intermediate crack-induced debonding in RC beams and slabs, Constr. Build. Mater. 17(6) (2003) 447-462.
[51] X.Z. Lu, J.G. Teng, L.P. Ye, J.J. Jiang, Bond–slip models for FRP sheets/plates bonded to concrete, Eng. Struct. 27(6) (2005) 920-937.
[52] H. Said, Z. Wu, Evaluating and proposing models of predicting IC debonding failure, J. Compos. Constr. 12(3) (2008) 284-299.
[53] Z. WU, H. NIU, Prediction of crack-induced debonding failure in R/C structures flexurally strengthened with externally bonded FRP composites, Doboku Gakkai Ronbunshuu E 63(4) (2007) 620-639.
[54] H. Elsanadedy, H. Abbas, Y. Al-Salloum, T. Almusallam, Prediction of intermediate crack debonding strain of externally bonded FRP laminates in RC beams and one-way slabs, J. Compos. Constr. 18(5) (2014) 04014008.
[55] X. Huang, L. Sui, F. Xing, Y. Zhou, Y. Wu, Reliability assessment for flexural FRP-Strengthened reinforced concrete beams based on Importance Sampling, Composites Part B: Engineering 156 (2019) 378-398.
[56] G. Carta, F. Stochino, Theoretical models to predict the flexural failure of reinforced concrete beams under blast loads, Eng. Struct. 49 (2013) 306-315.
[57] H.A. Rasheed, H. Charkas, H. Melhem, Simplified nonlinear analysis of strengthened concrete beams based on a rigorous approach, J. Struct. Eng. 130(7) (2004) 1087-1096.